Supporting Information

Electron Injection Promoted High-Efficient Electrocatalyst of $FeNi_3$@GR@Fe-NiOOH for Oxygen Evolution and Rechargeable Metal-air Batteries

Xin Wang[a,b], *Xiangye Liu*[a], *Chuan-Jia Tong*[c], *Xiaotao Yuan*[a], *Wujie Dong*[a], *Tianquan Lin*[b]*, *Li-Min Liu*[c]* and *Fuqiang Huang*[a,b]*

[a] State Key Laboratory of Rare Earth Materials Chemistry and Applications and Beijing National Laboratory for Molecular Sciences, College of Chemistry and Molecular Engineering, Peking University, Beijing 100871, P.R. China.

[b] CAS Key Laboratory of Materials for Energy Conversion, Shanghai Institute of Ceramics, Chinese Academy of Sciences, Shanghai 200050, P.R. China.

[c] Beijing Computational Science Research Center, Beijing 100094, P.R. China.

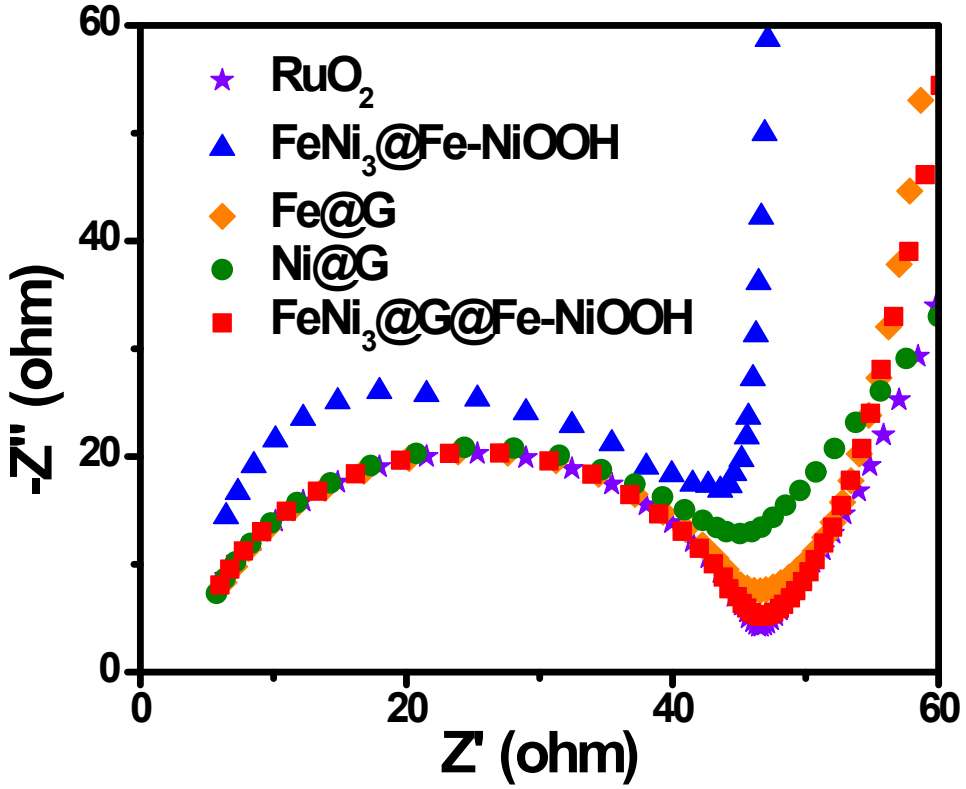

Figure S1. Nyquist plots of $FeNi_3$@GR@Fe-NiOOH, Fe@GR, Ni@GR, $FeNi_3$@Fe-NiOOH and RuO_2.

Table S1. The theoretical thickness and work functions of different layers of β-NiOOH on Ni

Number of NiOOH layers	1	2	3	4
Thickness of NiOOH layers (nm)	0.281	0.759	1.202	1.662
Work function (eV)	6.76	7.49	7.61	7.94

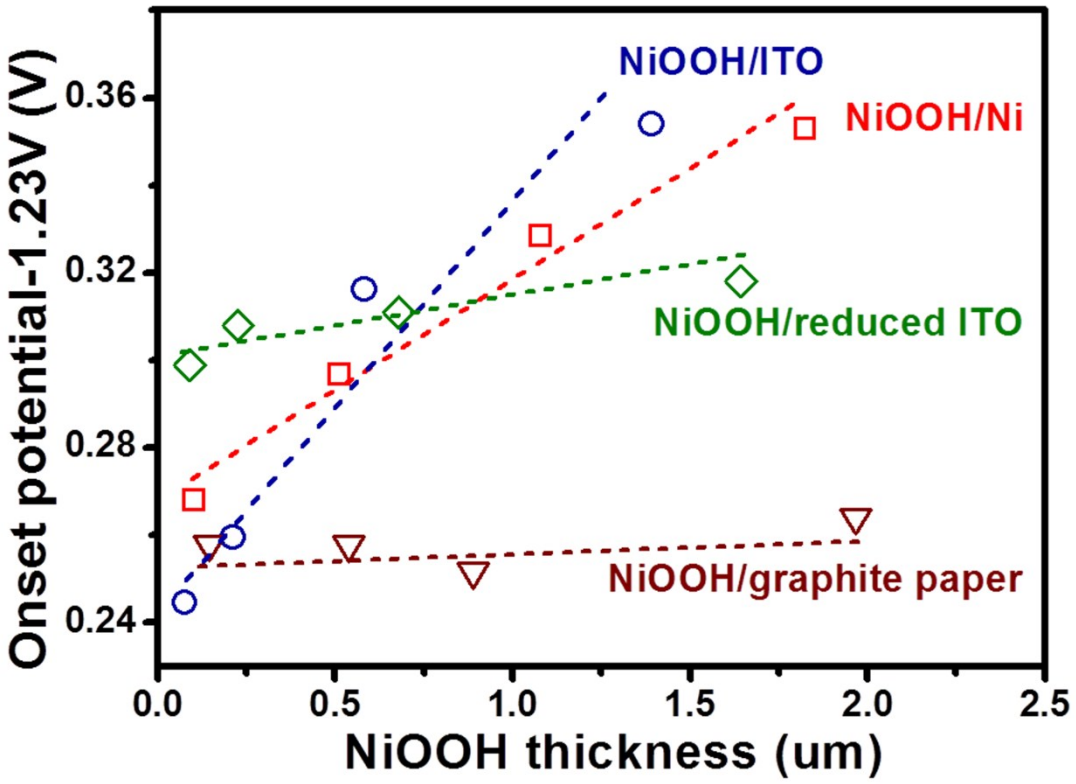

Figure S2. Function of the onset potential to NiOOH film thickness for NiOOH/Ni, NiOOH/ITO, NiOOH/reduced ITO and NiOOH/graphite paper.

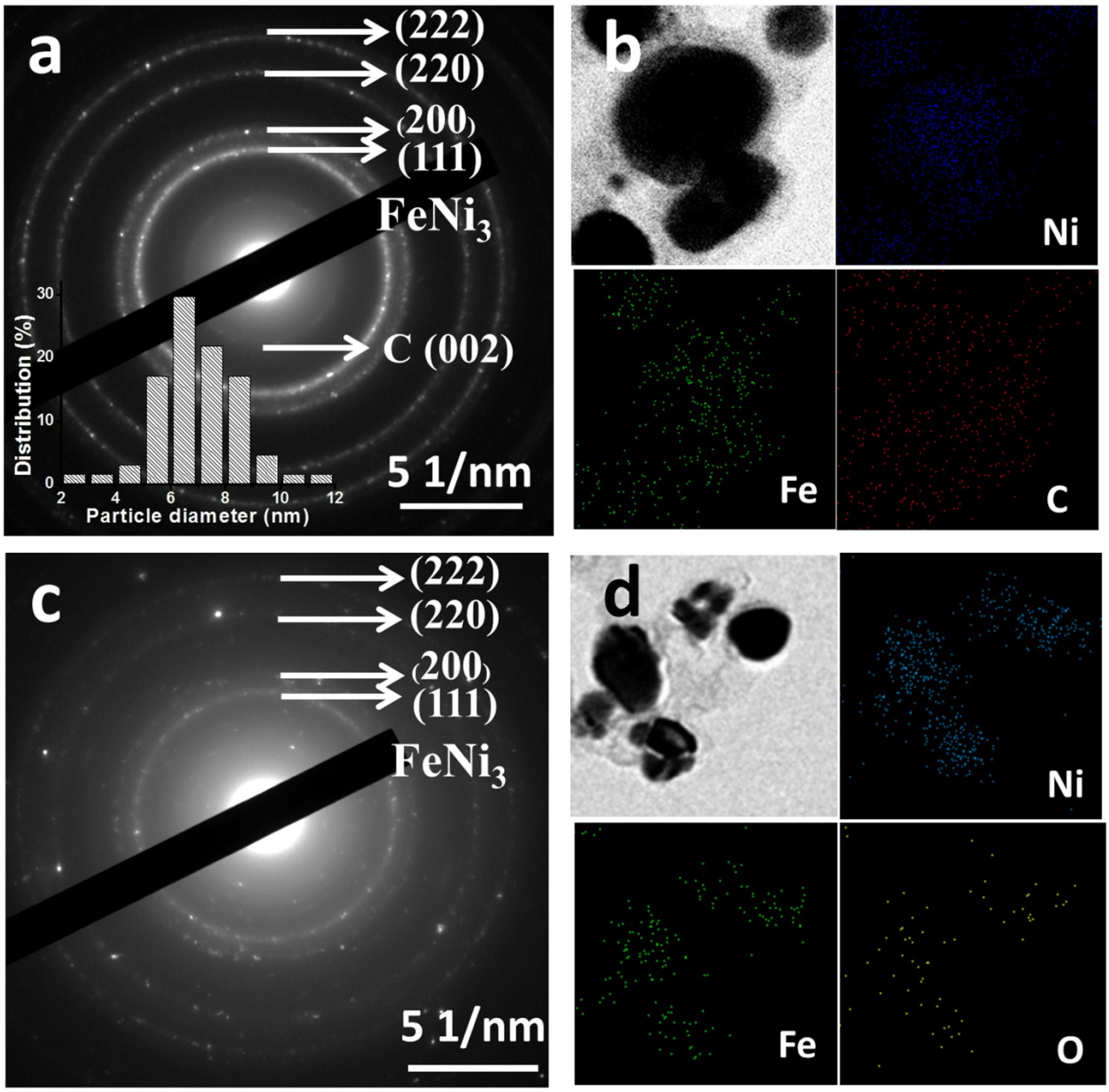

Figure S3. (**a**) Selected area electron diffraction (SAED) pattern of $FeNi_3$@GR. Inset: particle diameter histogram; (**b**) HAABF-STEM image of as-prepared $FeNi_3$@GR and EDX maps for Ni, Fe, C; (**c**) Selected area electron diffraction (SAED) pattern of $FeNi_3$@GR@Fe-NiOOH; (**d**) HAABF-STEM image of $FeNi_3$@GR@Fe-NiOOH and EDX maps for Ni, Fe, O.

Table S2. The work functions of Fe-NiOOH, $FeNi_3$, $FeNi_3$@GR, $FeNi_3$@Fe-NiOOH, $FeNi_3$@GR@Fe-NiOOH

Item	Fe-NiOOH	$FeNi_3$	$FeNi_3$@GR	$FeNi_3$@Fe-NiOOH	$FeNi_3$@GR@Fe-NiOOH
Work function(eV)	5.61	4.98	4.81	5.06	5.03

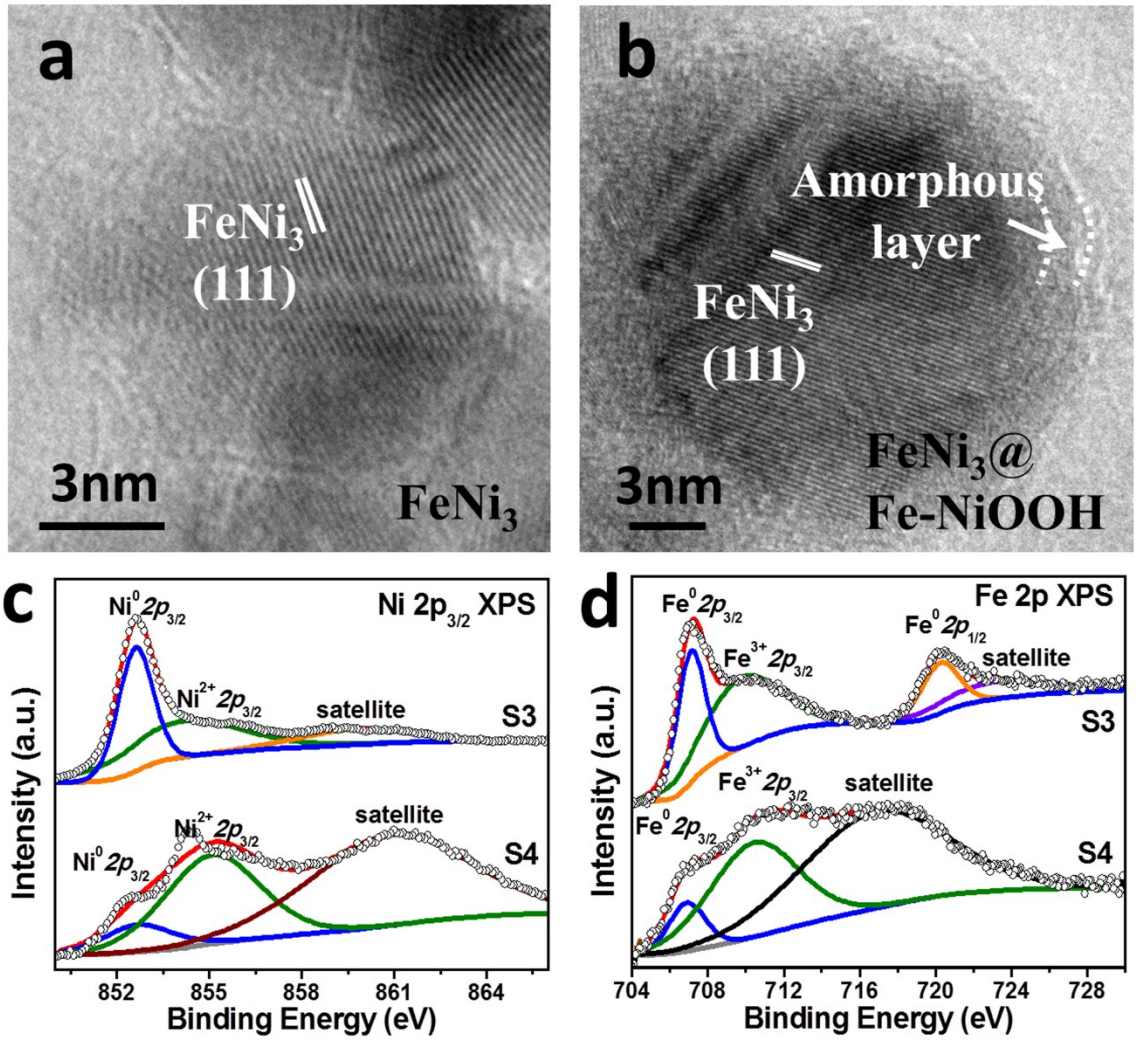

Figure S4. (**a**) Low magnification TEM image of $FeNi_3$(S3). Inset: HRTEM image of it and particle diameter histogram; (**b**) Low magnification TEM image of $FeNi_3$@Fe-NiOOH (S4). Inset: HRTEM image of it; XPS spectra of Ni $2p_{3/2}$ (**c**) and Fe 2p (**d**) of $FeNi_3$ (S3) and $FeNi_3$@Fe-NiOOH (S4).

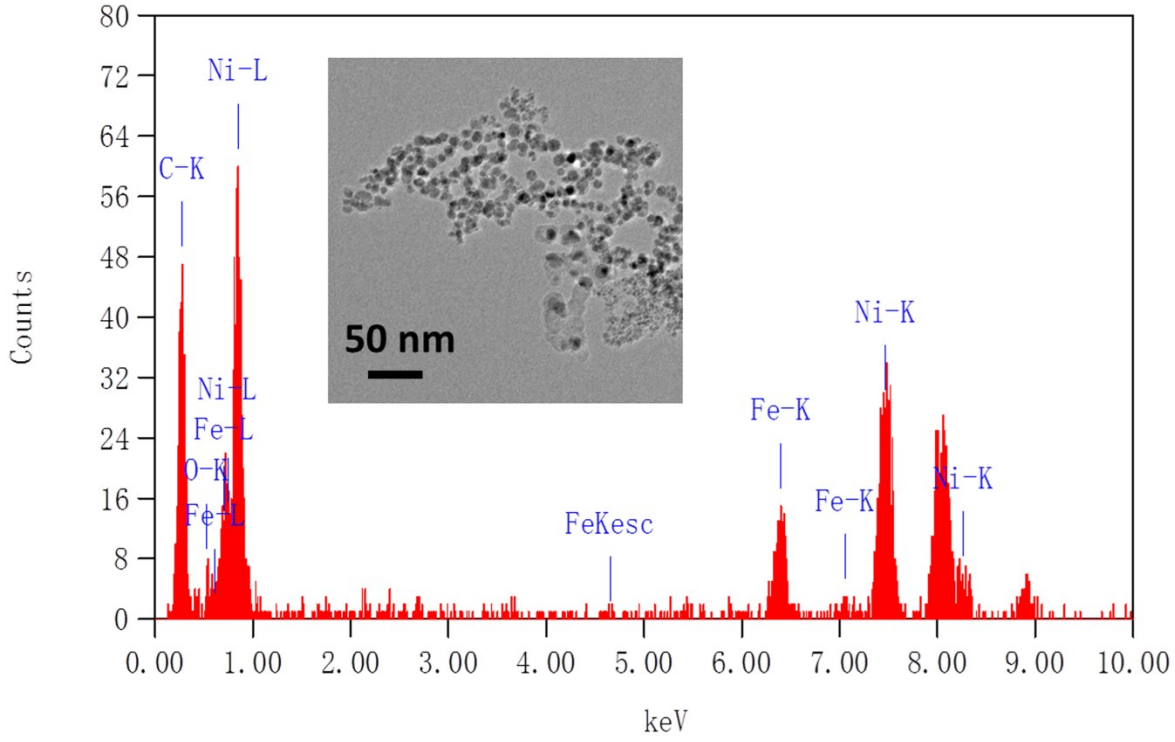

Figure S5. The energy dispersive X-ray spectroscopy of $FeNi_3$@GR@Fe-NiOOH; Inset: the TEM image of corresponding $FeNi_3$@GR@Fe-NiOOH.

Table S3. The elements content of $FeNi_3$@GR@Fe-NiOOH by EDS.

Element	(keV)	Mass%	Counts	Error%	Atom%
Ni K	7.471	1.18	22.28	0.18	7.58
Fe K	6.398	8.07	173.93	0.06	2.41
O K	0.525	26.72	511.78	0.02	1.23
C K	0.277	64.03	510.71	0.00	88.78

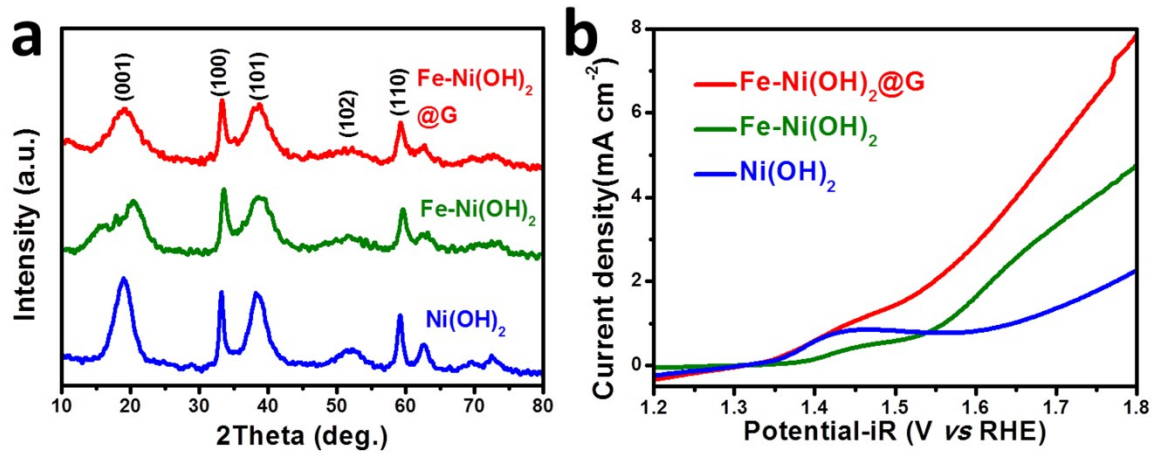

Figure S6. (a) XRD patterns of $Ni(OH)_2$, Fe-$Ni(OH)_2$ (5% Fe-doping content) and Fe-$Ni(OH)_2$@G (5% Fe-doping content); (b) Polarization curve of $Ni(OH)_2$, Fe-$Ni(OH)_2$ and Fe-$Ni(OH)_2$@G (loading mass: 0.25 mg cm^{-2}) collected at 10 mV s^{-1} and 2,000 rpm in O_2-saturated 0.1 M KOH.

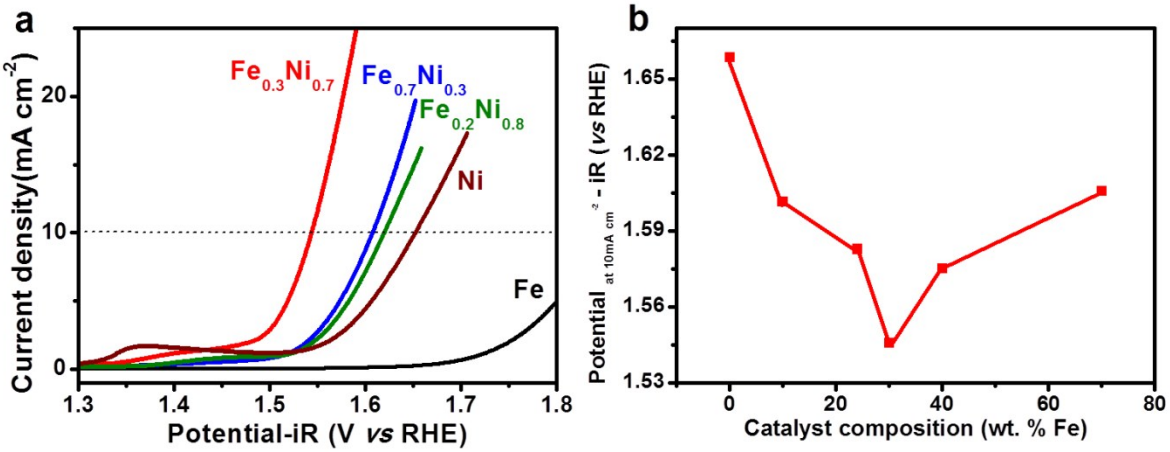

Figure S7. (a) Polarization curve of Fe_xNi_y@GR@Fe-NiOOH of different ratio of Fe and Ni (loading mass: 0.25 mg cm^{-2}) collected at 50 mV s^{-1} and 2000 rpm in O_2-saturated 0.1 M KOH. According to the order from more to less of Ni, the ratios of Fe and Ni were 0:10, 2:8, 3:7, 7:3 and 10:0. (b) The plot of potential at 10 mA cm^{-2} of different Fe_xNi_y@GR@Fe-NiOOH samples with the content of Fe in catalysts.

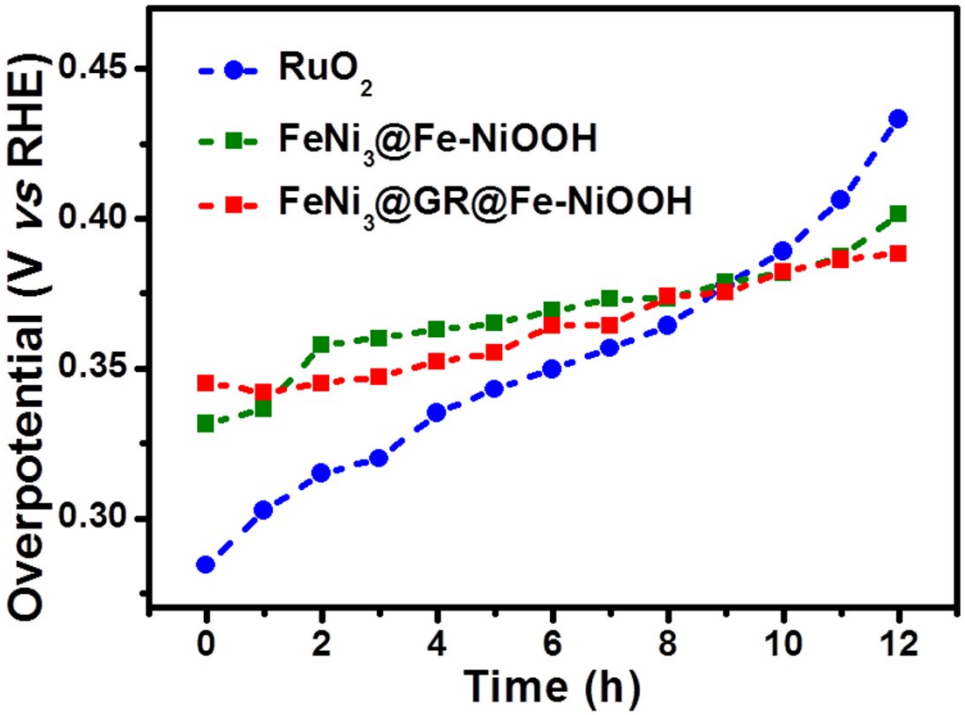

Figure S8. Plots of overpotential as a function of time for $FeNi_3$@GR@Fe-NiOOH, $FeNi_3$@Fe-NiOOH and RuO_2 recorded under a 5 mA cm^{-2} constant current density at 2000 rpm in O_2-saturated 0.1 M KOH.

Equation 1-5. Reaction pathway for oxygen evolution in alkaline solutions

$$S + OH^- \rightarrow S\text{-}OH + e^- \quad (1)$$

{b = 2.3*(2RT/F) = 120 mV/dec}

$$S\text{-}OH + OH^- \rightarrow S\text{-}O^- + H_2O \quad (2)$$

{b = 2.3*(RT/IF) = 60 mV/dec}

$$S\text{-}O^- \rightarrow S\text{-}O + e^- \quad (3)$$

{b = 2.3*(2RT/3F) = 40 mV/dec}

$$2S\text{-}O \rightarrow 2S + O_2 \quad (4)$$

{b = 2.3*(RT/4F) = 15 mV/dec}

where S is an active site in the catalyst, and b represents the Tafel slope (values shown are at room temperature).

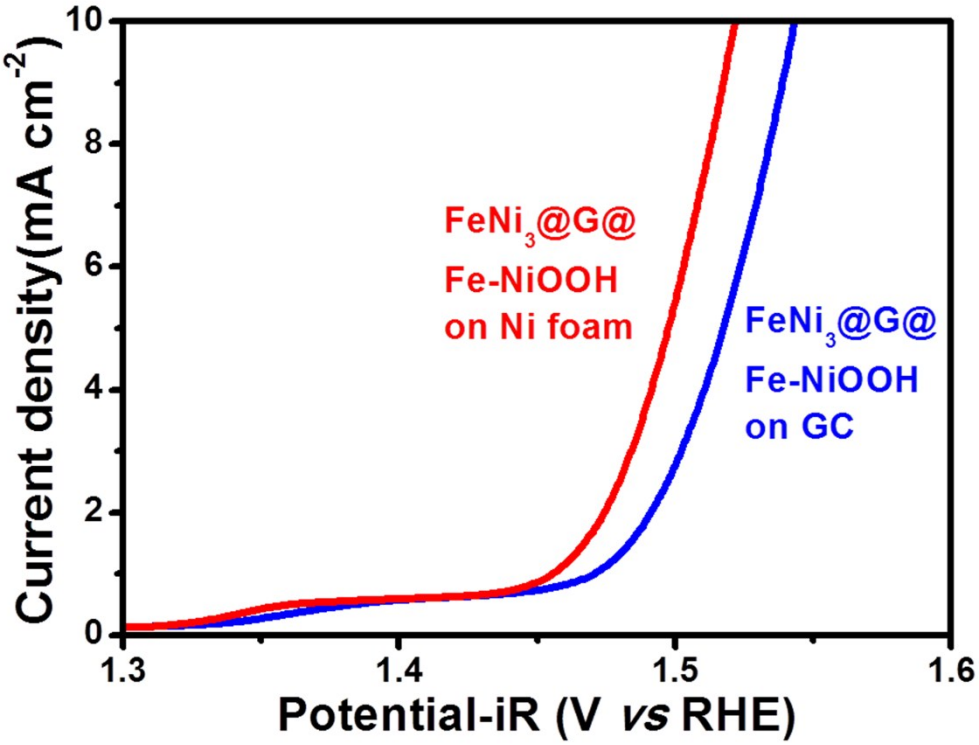

Figure S9. Polarization curve of $FeNi_3$@GR@Fe-NiOOH on Ni foam and $FeNi_3$@GR@Fe-NiOOH on glassy carbon electrode (loading mass: 0.25 mg cm^{-2}) collected at 10 mV s^{-1} in O_2-saturated 0.1 M KOH.

Table S4. Comparison of OER performance of recent Ni-based OER catalysts

Sample	Onset η (V)	η at 10 mA cm^{-2} (V)	TOF at 0.3V (s^{-1})	Tafel slope (mV dec^{-1})	Durability	Ref.
$FeNi_3$@GR@Fe-NiOOH	0.22	0.29	1.16	65	No change in 12 h	/
$Ni_{0.9}Fe_{0.1}O_x$ film	0.23	0.34	0.21	30	/	[1]
Ni-Fe LDH nanosheet	0.25	0.32	0.05	67(bulk)	/	[2]
$Ni_{0.69}Fe_{0.31}O_x$/C	0.25	0.28	0.20	30	No change in 2 h	[3]
Fe-doped $Ni(OH)_2$/NiOOH	0.23	0.29	0.82	37	/	[4]
FeNi-rGO-LDH hybrids	0.20V	0.22V	0.987	39	No change in 1.5 h	[5]
FeNi@NC	0.21	0.28		70		[6]

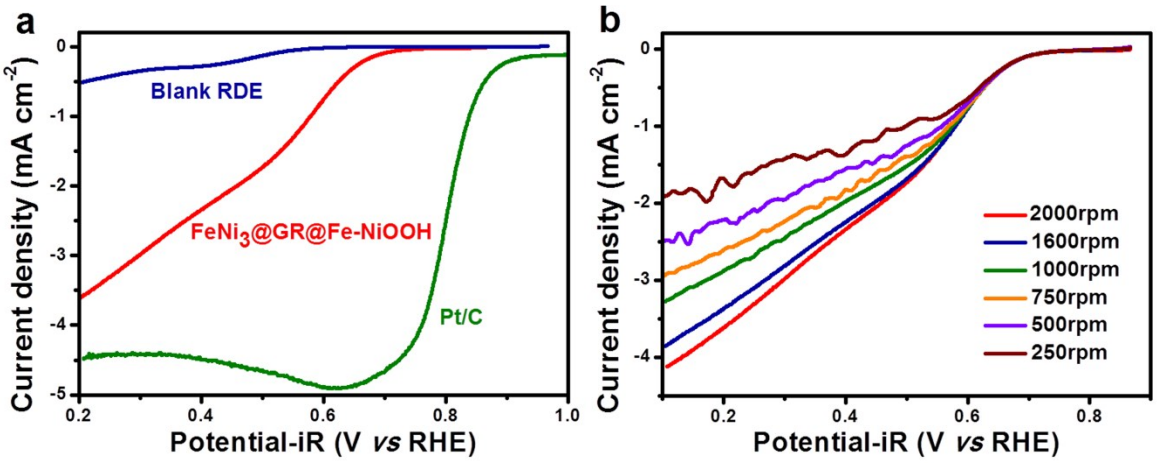

Figure S10. (a) Polarization curve of $FeNi_3$@GR@Fe-NiOOH, blank RDE and Pt/C (mass loading: 0.25mg cm^{-2}) collected at 10 mV s^{-1} and 1600 rpm in O_2-saturated 0.1 M KOH; (b) Polarization curve of different rotational speed to $FeNi_3$@GR@Fe-NiOOH (mass loading: 0.25mg cm^{-2}) collected at 10 mV s^{-1} in O_2-saturated 0.1 M KOH.

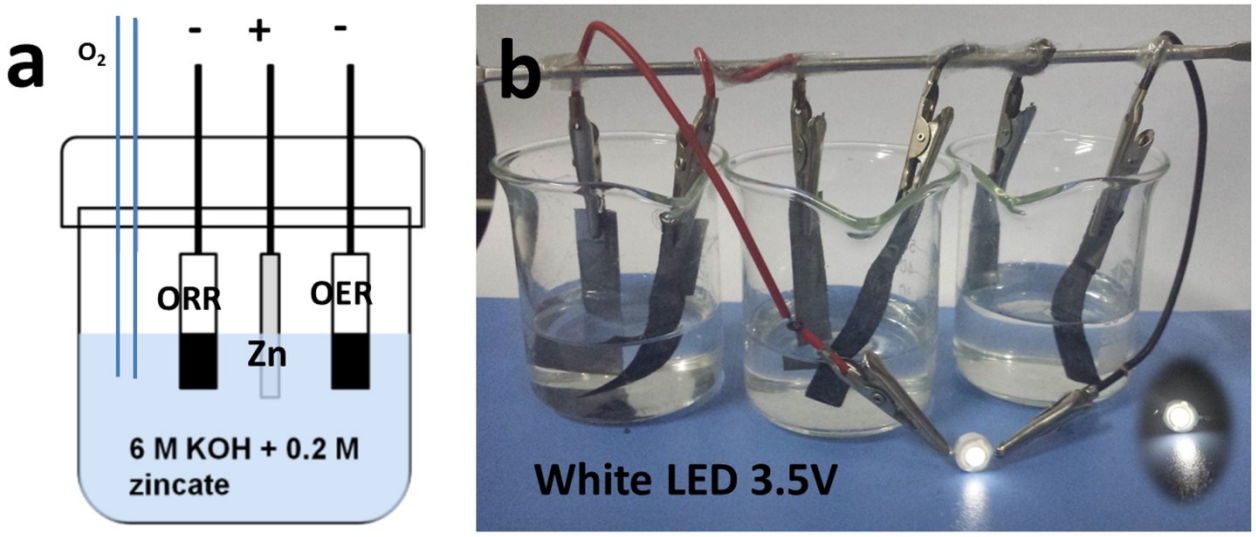

Figure S11. (**a**) Schemic illustration for a three-electrode rechargeable Zn-air battery using $FeNi_3$@GR@Fe-NiOOH and Pt/C as OER and ORR catalysts. (**b**) Optical images of LED powered by three home-made Zn-air batteries in series; Inset: optical image of LED in dark.

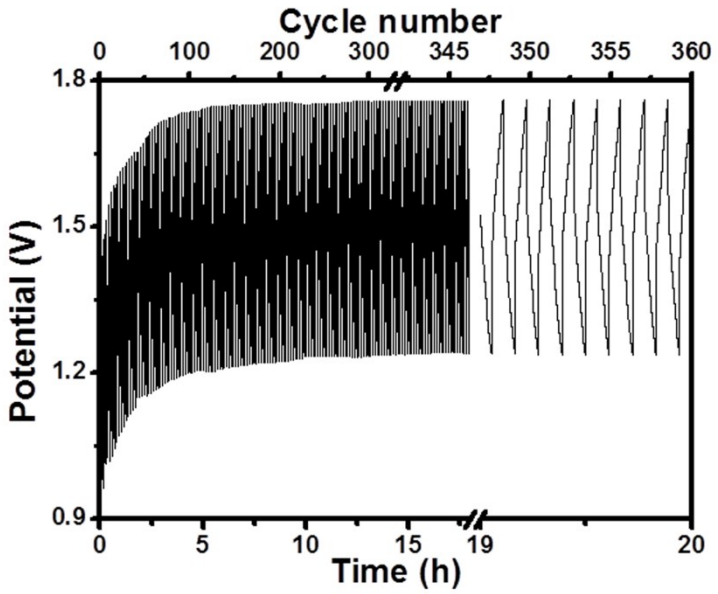

Figure S12. Discharge/charge cycling curves of a two-electrode Zn-air battery using a mix of Pt/C and RuO_2 as catalyst (0.5 mg cm^{-2} for OER and 0.1 mg cm^{-2} for ORR) at a current density of 1 mA cm^{-2}.

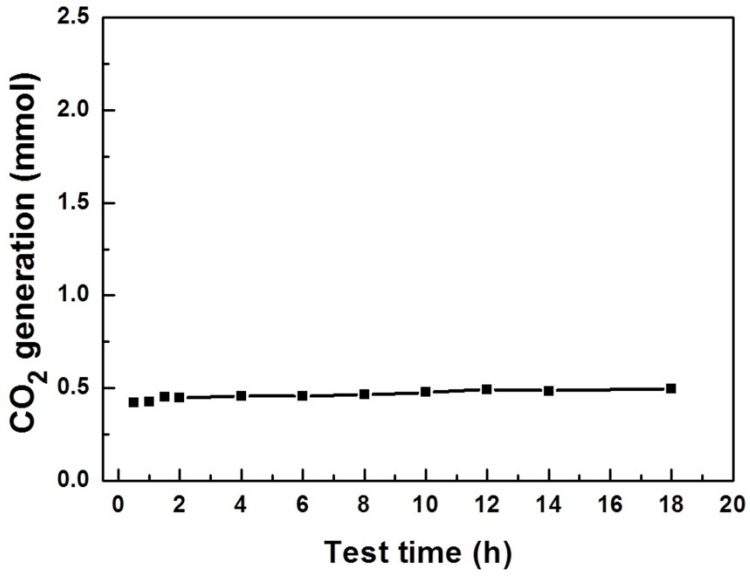

Figure S13. CO_2 generation of $FeNi_3$@GR@Fe-NiOOH in the course of OER catalysis by the gas chromatography for 12 hours.

Reference:

[1] Lena Trotochaud, James K. Ranney, Kerisha N. Williams, and Shannon W. Boettcher Solution-Cast Metal Oxide Thin Film Electrocatalysts for Oxygen Evolution. *J. Am. Chem. Soc.* 2012, 134, 17253−17261.

[2] Fang Song, Xile Hu. Exfoliation of layered double hydroxides for enhanced oxygen evolution catalysis. *Nat. Commun.* 5:4477.

[3] Yang Qiu, Le Xin, and Wenzhen Li. Electrocatalytic Oxygen Evolution over Supported Small Amorphous Ni−Fe Nanoparticles in Alkaline Electrolyte. *Langmuir* 2014, 30, 7893−7901.

[4] Mary W. Louie and Alexis T. Bell. An Investigation of Thin-Film Ni−Fe Oxide Catalysts for the Electrochemical Evolution of Oxygen. *J. Am. Chem. Soc.* 2013, 135, 12329−12337.

[5] Xia Long, Jinkai Li, Shuang Xiao, Keyou Yan, Zilong Wang, Haining Chen, and Shihe Yang. A Strongly Coupled Graphene and FeNi Double Hydroxide Hybrid as an Excellent Electrocatalyst for the Oxygen Evolution Reaction. *Angew. Chem. Int. Ed.* 2014, 53, 7584-7588.

[6] Xiaoju Cui, Pengju Ren, Dehui Deng, Jiao Deng and Xinhe Bao. Single layer graphene encapsulating non-precious metals as high-performance electrocatalysts for water oxidation. *Energy Environ. Sci.,* 2016, 9, 123